



POLİTEKNİK DERGİSİ

JOURNAL of POLYTECHNIC

ISSN: 1302-0900 (PRINT), ISSN: 2147-9429 (ONLINE)

URL: <http://dergipark.gov.tr/politeknik>



# Selection of excitation operating points of 10 MW HTS exciting double stator direct-drive wind generators having single and double polarity inner stator

*Tek ve çift kutuplu iç statorlu olan 10 MW HTS tahrikli çift statorlu doğrudan tahrikli rüzgâr jeneratörlerinin uyarma çalışma noktalarının seçimi*

*Yazar(lar) (Author(s)):* Ming CHENG<sup>1</sup>, Xinfu NING<sup>2</sup>, Xinkai ZHU<sup>3</sup>, Yubin WANG<sup>4</sup>

*ORCID<sup>1</sup>:* 0000-0002-3466-234X

*ORCID<sup>2</sup>:* 0000-0002-3211-8017

*ORCID<sup>3</sup>:* 0000-0001-5399-8191

*ORCID<sup>4</sup>:* 0000-0002-6732-2464

**Bu makaleye şu şekilde atıfta bulunabilirsiniz (To cite to this article):** Cheng M., Ning X., Zhu X., Wang Y., “Selection of excitation operating points of 10 MW HTS exciting double stator direct-drive wind generators having single and double polarity inner stator”, *Politeknik Dergisi*, 23(2): 537-545, (2020).

**Erişim linki (To link to this article):** <http://dergipark.gov.tr/politeknik/archive>

**DOI:** 10.2339/politeknik.605750

# Tek ve Çift Kutuplu İç Statorlu Olan 10 MW HTS Tahrikli Çift Statorlu Doğrudan Tahrikli Rüzgâr Jeneratörlerinin Uyarma Çalışma Noktalarının Seçimi

*Araştırma Makalesi / Research Article*

Ming CHENG<sup>1\*</sup>, Xinfu NING<sup>1</sup>, Xinkai ZHU<sup>1</sup>, Yubin WANG<sup>2</sup>

<sup>1</sup>School of Electrical Engineering, Southeast University, Nanjing 210096, China

<sup>2</sup>College of Information and Control Engineering, China University of Petroleum, Qingdao, China

(Geliş/Received : 16.08.2019 ; Kabul/Accepted : 28.01.2020)

## ÖZ

Yüksek sıcaklık süper iletkenliği (HTS) tahrikli çift stator olan doğrudan tahrikli rüzgâr jeneratörü (HTS-DSDDG), çift stator yapısı kullanılarak soğutma sisteminin statik sızdırmazlığını ve akımın fırçasız aktarmasını eşzamanlı olarak sağlayabilmekte olduğu için açık deniz rüzgâr jenerasyonunun gelecek vadeden bir yöntemidir. Bu çalışmada, sırasıyla tek kutuplu uyarma ve çift kutuplu uyarma olarak belirlenmek olan, HTS bobininin iki çeşit yerleştirme stratejisi önerilmektedir. Üstelik, HTS bobininin uyarma çalışma noktalarını belirlemek için bu çalışmada HTS kablolarının tüketimi ile tek/çift kutuplu HTS-DSDDG'lerin hacmi arasındaki ilişki kantitatif olarak araştırılmaktadır. HTS bobinlerinin farklı yerleştirme stratejileri, uyarma çalışma noktalarının, jeneratör boyutlarının ve HTS kabloları tüketiminin farklarına neden olacağından dolayı tek ile çift kutuplu HTS-DSDDG elektromanyetik verimi, ağırlığı ve malzeme masrafı açısından karşılaştırılmaktadır. Sonuç olarak, çift kutuplu HTS-DSDDG'nin tek kutuplu HTS-DSDDG'den daha hafif ve daha düşük maliyetli olduğu çıkarılmaktadır.

**Anahtar Kelimeler:** Büyük ölçekli rüzgâr jeneratörü, HTS, çift stator, Çift statorlu, uyarma çalışma noktası.

# Selection of Excitation Operating Points of 10 MW HTS Exciting Double Stator Direct-Drive Wind Generators Having Single and Double Polarity Inner Stator

## ABSTRACT

The high temperature superconducting (HTS) exciting double stator direct-drive wind generator (HTS-DSDDG) is a promising approach for offshore wind generation, due to the fact that double-stator structure is employed to simultaneously realize stationary seal of the cooling system and brushless of current transfer. In this paper, two kinds of placement strategies of HTS coils are proposed, denoted as single-polarity excitation and double-polarity excitation, respectively. Furthermore, the relationship between the consumption of HTS wires and the volume of the single-/double-polarity HTS-DSDDGs is quantitatively investigated to determine the excitation operating points of HTS coils. Since the different placement strategies of HTS coils will lead to differences of the excitation operating points, as well as differences of generator size and HTS wires consumption, the single-/double-polarity HTS-DSDDGs are compared in terms of the electromagnetic performance, the weight and the material cost. Finally, the conclusion is drawn that the 10 MW double-polarity HTS-DSDDG is lighter and lower cost than the single-polarity one.

**Keywords:** Large-scale wind generator, HTS, double-stator, direct-drive, excitation operating point.

## 1. INTRODUCTION

In recent decades, wind power generation has become one of the most attractive and competitive methods of renewable power generation [1-4], of which offshore wind power generation is rapidly developing due to harvest wind resource and sufficient space in sea, and considered to play a major role in contributing to renewable power generation in the future [5,6]. At the end of 2018, the total global installed capacity of offshore wind power generation exceeded 23 GW, and it is projected to reach 100 GW in 2025 [7]. Generally, larger wind turbines can lead to the lower average Levelized

Cost of Energy (LCOE), so the larger power wind turbines are becoming a development trend of the offshore wind power generation [5]. In 2018, the average rated capacity of European newly-installed offshore wind turbines was 6.8MW, a 15% increase over 2017 [8], and this number is expected to increase to 8 MW by 2020 [9]. At present, the 10 MW or above wind turbine with acceptable size and weight is research hotpot in both industrial and academic communities [10,11]. However, wind turbines face many challenges and limitations with the capacity increase, one of which is the electromechanical conversion system, i.e. drive train of wind turbine.

There are three general technology routes employed in the drive train of wind turbines [11,12,13]: 1) A three-

\*Sorumlu yazar (Corresponding Author)  
e-posta: mcheng@seu.edu.cn

stage gearbox is combined with a high speed induction generator, i.e. Gear-drive train; 2) A single/two-stage gearbox is combined with a medium-speed synchronous generator, i.e. semi-direct-drive train; 3) A rotor is directly connected to a low-speed synchronous generator without the gearbox, i.e. direct-drive train. However, the numerous rotating parts and bearings in gearbox will result in its unreliability, and gearbox requires frequent maintenance, resulting in undesired downtime [13]. Since there are strict environmental restrictions at the offshore wind farms, Gearbox maintenance is costly, and gearbox failure will cause significant losses. In addition, the weight of the gearbox increases with the rated capacity of wind turbine, increasing the load on structural support. While the direct-drive train using the low-speed generator eliminates the gearbox from the turbine drive-train, offering the merits of lighter weight, lower maintenance cost, and higher reliability, compared with the geared-train and the semi-direct-drive train, it has become the preferable option for large offshore wind turbine [11]. Obviously, the low-speed generator is one of the most critical components of the direct-drive train. The electrically excited synchronous generator (EESG) and permanent magnet synchronous generator (PMSG) are the two main options for direct-drive trains. However, the size and weight of 10 MW low speed EESGs or PMSGs are very huge, which makes their construction, transportation and installation to be significantly difficult and cost rising, resulting in hardly meeting the requirement of the offshore wind generation [14]. Besides, the price of permanent magnets is subject to the risk of fluctuation. Luckily, the use of superconducting (SC) materials in low speed wind generators named as superconducting direct-drive synchronous generator (SCDDG), emerges as a promising solution for achieving reliable, lightweight, and higher power level (10 MW or beyond) wind turbine [15,16].

At present, lots of research on SCDDGs are being actively carried out [17-27]. In [18], various topologies of SCDDGs were reviewed. In [19], comparative assessment of Multi-Megawatt Class SCDDGs was made, showing that the economy of SCDDGs improves with the rating increase, they are superior to PM direct-drive generators (PMDDGs) when the rating is above 8 MW. However, the 10 MW existing conceptual SCDDGs face the challenges of rotating sealing of the cooling system or the brush-slip ring system for conducting large armature current, which probably results in the low reliability, manufacturing difficulty and high cost. In order to solve these problems faced by the existing conceptual SCDDGs, a 10 MW novel HTS exciting double stator direct-drive wind generator (HTS-DSDDG) was proposed to simultaneously realize stationary seal of the cooling system and brushless of current transfer, showing a promising prospect in the offshore wind generation [17].

The HTS winding used in HTS-DSDDG permits the achievement of much stronger magnetic loading than that of the EDDG and PMDDG, bring the possibility of

smaller size and lighter weight. The existing design cases of SCDDGs indicate that the high cost of SC materials is a major factor of limiting the application of SCDDGs. Therefore, it is indispensable to study the relationship between the consumption of HTS material and the size of HTS-DSDDG, which is of great significance to reduce the cost of wind power generation. The consumption of HTS material is determined by the turn number and the size of HTS winding, while the size of HTS winding mainly depends on the geometry and the size of HTS-DSDDG. The turn number of HTS field winding and the magnitude of field current, i.e. the excitation operating point, affect the magnetic loading and power density of the generator, hence the geometry design of HTS-DSDDG must be coordinated with the excitation operating point to achieve a power rating of 10 MW. Generally, the higher excitation-MMF (multiply the turn number of HTS winding by the field current), the higher magnetic loading and the smaller the size of the generator, but this is limited by the saturation effect of magnetic material. Besides, the field current of HTS winding is limited by the magnetic field, which complicates the relationship between these variables. However, the problem can be simplified by fixing the cross-section of geometry of the generator. In this case, the magnetic field of HTS-DSDDG is substantially determined at a certain excitation-MMF, so the field current and the turn number of the HTS winding can be calculated. Different excitation operating points correspond to different field currents and HTS winding turns, different magnetic loading and power density of the generator, different active axial lengths of the generator, and different consumption of HTS materials. Therefore, the HTS material consumption and the size of HTS-DSDDG depend on the excitation operating point in the case of this paper.

In this paper, a method of determining the excitation operating point of the HTS-DSDDG is proposed, and based on this, two 10 MW conceptual HTS-DSDDGs with different placement strategies of HTS coils are analyzed and compared. In Section 2, the structure and operating principle of the HTS-DSDDG are discussed. In Section 3, the method of determining the excitation operating point of the HTS-DSDDG is described in detail using the finite element analysis (FEA). Then the electromagnetic performance, the weight and the material cost of the two conceptual HTS-DSDDGs are compared in Section 4. Finally, some conclusions are drawn in Section 5.

## 2. STRUCTURE AND OPERATING PRINCIPLE

### 2.1. Structure

The cross section of the single-/double-polarity HTS-DSDDGs are shown in Figure 1. It can be seen that the HTS-DSDDG mainly consists of an outer stator with copper armature winding, a sandwiched reluctance-rotor between two stators, and an inner stator with racetrack-shaped cryogenic dewars containing HTS coils, from the

outside to the inside. The main difference between the single-polarity and double-polarity HTS-DSDDG is the placement strategy of HTS coils on the inner stator. For the double-polarity one, there is one dewar on each inner-stator-tooth, and the polarities of the two HTS windings in adjacent dewars are opposite, as shown in Figure 1(a), in which the red arrows indicate N poles and the blue arrows indicate S poles. So two adjacent dewars combine an excitation pole-pair. While for the single-polarity one, the polarities of all HTS windings are the same, i.e., N poles or S poles, between which iron consequent poles are sandwiched, as shown in Figure 1(b), so one dewar and an adjacent iron pole combine an excitation pole-pair. Although the number of dewar of the single-polarity one is only half of that of the double-polarity counterpart, the equivalent pole-pair number of them are the same, i.e., equal to the number of the magnetic-block of rotor. However, since each inner-stator-slot contains two dewar edges in the double-polarity one, while only one dewar edge in the single-polarity one, the width of inner-stator-teeth of the double-polarity one is slightly smaller than that of the single-polarity one.

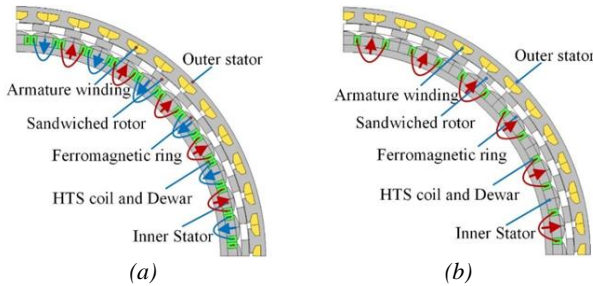


**Figure 1.** Cross section of the HTS-DSDDGs with different excitation structures: (a) double polarity, (b) single polarity.

## 2.2. Operating Principle

According to the airgap field modulation theory (AFMT) for electrical machines [28], the fundamental magnetic field excited by the HTS windings on inner stator will be modulated by the rotating sandwiched reluctance-rotor. Then abundant of rotating and stationary harmonics will be generated in the outer airgap after the modulation, of which the harmonics having the same order, rotating speed, and rotating direction as those of armature reaction can interact with each other to output constant electromagnetic torque. The corresponding number of pole pairs  $P_j$  and rotating speed  $n_j$  of the harmonics in the outer airgap can be obtained by:

$$P_j = |P_{HTS} - jN_{Fe}| \quad (1)$$

$$n_j = \frac{jN_{Fe}}{jN_{Fe} - P_{HTS}} n_r \quad (2)$$

where  $n_r$  is the rotor speed,  $N_{Fe}$  is the number of magnetic-block of rotor, and  $P_{HTS}$  is the pole-pair number of the fundamental magnetic field in the inner airgap,  $j = 0, \pm 1, \pm 2, \dots, \pm \infty$ .

The existing research results show that the main effective harmonic corresponds to the case of  $j = 1$ . Therefore, the pole-pair number and the rotating speed of the main effective magnetic-field harmonic for the HTS-DSDDGs with 44-rotor-magnetic-block and 24-pole-pair of fundamental magnetic field, i.e.,  $N_{Fe} = 44$  and  $P_{HTS} = 24$ , can be derived as  $P_1 = 20$  and  $n_1 = 2.2n_r$ . Hence the frequency  $f_1$  of the EMF can be calculated by:

$$f_1 = \frac{n_1 P_1}{60} = \frac{2.2n_r \cdot 20}{60} = \frac{44n_r}{60} \quad (3)$$

## 3. SELECTION OF EXCITATION OPERATING POINT

The torque density of electrical machine is proportional to the magnetic loading  $B$  and the electrical loading  $A$ , meaning that the higher  $B$  or  $A$ , the smaller size and lighter weight for electrical machine. Although the use of HTS field coils in the HTS-DSDDG permits the achievement of much stronger excitation-MMF due to the high DC capacity of HTS coils without joule loss, the increase of the  $B$  is not linear with the increase of the excitation-MMF due to the saturation effect of magnetic material, such as silicon steel used in stator yoke or teeth. Therefore, when the saturation of silicon steel reach to a certain level, it would not be an effective method to continuously increase the torque density by continuously increasing the excitation-MMF to acquire a higher  $B$ , due to the fact that a lot of HTS wires will be needed to get a very little increase of torque density under the condition of high saturation. Besides, the maximum flux density perpendicular to the HTS coil will be increased as the increase of the excitation-MMF, resulting in the reduce of the critical engineering current of HTS coil and the increase of consumption of HTS wire, since the effect of the perpendicular flux density on the critical engineering current of HTS coil is very heavy. Generally, the higher perpendicular flux density, the lower critical engineering current. Hence, it is very important to determine a proper excitation operation point of the HTS coils for the HTS-DSDDG.

In this section, a selection method of excitation operating point is proposed, the specific steps are as follows:

- (1) The critical engineering current ( $I_{fmax}$ ) and the turn number of per excitation pole-pair ( $N_f$ ) is obtained under the different excitation-MMF per excitation pole-pair ( $F_c$ ) by analyzing the maximum flux density around the HTS coil using the method of FEA. So, the relationship of the  $I_{fmax}$ ,  $N_f$ , and  $F_c$  can be obtained.
- (2) The torque density of the HTS-DSDDG is compared under the different  $F_c$  with all geometric specifications fixed. Then the rotor axial length ( $l_{ap}$ ) is adjusted to achieve an output power of 10 MW, and the  $l_{ap}$ - $F_c$  curves are obtained.
- (3) The consumption of the HTS wire per excitation pole-pair ( $l_{HTS}$ ) can be obtained from the  $N_f$  of the step (1) and the specific geometric size under the

different  $F_c$ . Then the relationship of the  $I_{HTS}$  and  $l_{ap}$  can be obtained. Finally, the excitation operating point is determined from the  $l_{ap}$ - $I_{HTS}$  curves.

For single-polarity HTS-DSDDG, there is one edge of HTS winding in each inner-stator-slot, while there are two for double-polarity HTS-DSDDG, as shown in Figure 2. This leads to two results: 1) The widths of inner-stator-teeth of the two generators are different, so are the saturations of inner-stator-teeth and the torque capacities. 2) When  $F_c$  are the same, the magnetic fields in HTS winding area are different, hence the  $I_{fmax}$  and  $N_f$  of the two structures are different. Therefore, the different characteristics of the magnetic field in HTS winding area and the torque capacity lead to the difference of the excitation operating points. In order to fairly compare the single-/double-polarity HTS-DSDDG in detail, the excitation operation points of them will be determined by the aforementioned method. The main design specifications of the two HTS-DSDDGs are listed in Table 1, and more specific design considerations are illustrated in [17].

In order to simplify the magnetic-field analysis around the HTS coils, some assumptions are given as follows:

- (1) The flux density distribution in each inner-stator-slot is the same, so the magnetic field analysis is conducted for only one inner-stator-slot, and eight indicated points are built around the HTS coil, namely, point 1, 2, 3, 4, 5, 6, 7, and 8 (p1, p2, p3, p4, p5, p6, p7, and p8), as shown in Figure 2. The flux density of each indicated point denotes the flux density of the corresponding zone near the HTS coil.
- (2) The field current distribution in the HTS coil is homogenous, whose distribution zone shown in Figure 2 is highlighted in red color. Since the effect of the perpendicular applied field on the critical engineering current of HTS coil is heavier than that of the parallel applied field, the absolute value of flux density of the indicated points will be regarded as perpendicular field for safety margin. At the same time, it is assumed that the maximum of the field current ( $I_{fmax}$ ) in the HTS coil is determined by the maximum of flux density among the eight indicated points, according to the  $I_c$ - $B_{\perp}$  curve at 30 K considering 30% safety margin, namely, the  $I_{fmax}$ - $B_{\perp}$  curve, as shown in Figure 3, in which the  $I_c$  is the critical current of the Bi2223 in the condition of self-field and cooling temperature 30 K, and the  $I_c$ - $B_{\perp}$  curve is provided by the manufacturer (Innova Superconductor Technology Co. Ltd). The reason of selecting the cooling temperature of 30 K is described in detail in [29].
- (3) The total length of the HTS wire is equal to that the pole-pair number of excitation winding multiplies the length of HTS wire per excitation pole-pair. And the length of HTS wire per excitation pole-pair is assumed to be approximately that the length of middle turn of HTS coil multiplies the turn number per excitation pole-pair.

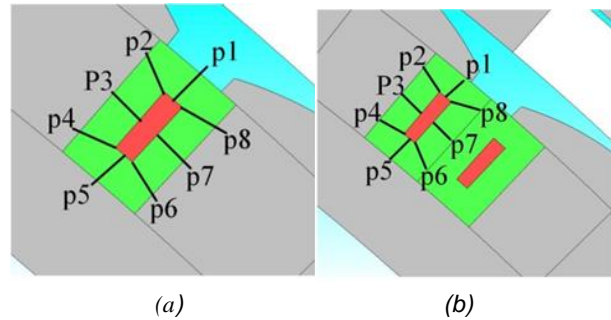


**Figure 2.** Eight indicated points around the HTS coil: (a) single-polarity, (b) double-polarity.

**Table 1.** The main design specifications of the HTS-DSDDG

Parameters	Symbol	Single-polarity	Double-polarity
Rated power (MW)	$P_N$	10	10
Rated rotating speed (r/min)	$n_N$	9.6	9.6
Rated torque (MN·m)	$T_N$	11	11
Line voltage of armature winding (Vrms)	$V_N$	4000	4000
phase current of armature winding (Arms)	$I_N$	2545	2545
Power factor	$\cos(\varphi)$	1	1
Number of cryogenic dewar	$N_D$	24	48
Armature winding configuration	-	3-phase	3-phase
Armature cooling method	-	forced air cooling	forced air cooling
Polarity of adjacent HTS field coils	-	same polarity	opposite polarity
Superconducting wire	-	Bi2223	Bi2223
Operation temperature of HTS coil (K)	$T_{oper}$	30	30
Width of inner-stator-teeth (mm)	$b_{ist}$	466	330

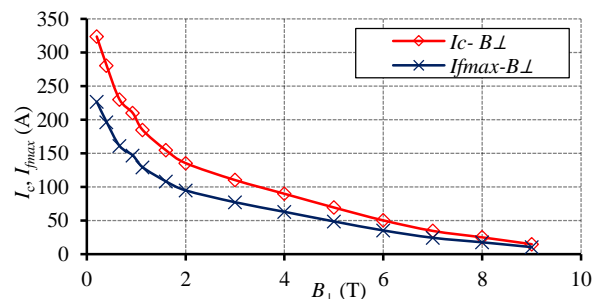


**Figure 3.**  $I_c$ - $B_{\perp}$  curve of Bi2223 wire and  $I_{fmax}$ - $B_{\perp}$  curve of HTS coil at the cooling temperature of 30 K.

In this section, the magnetic field analysis is studied by the FEA, it can be found that the magnitude of flux density at p1-p8 periodically changes with the rotor rotation, but the direction of which is almost unchanged.

Figure 4 shows the direct component and fundamental component of flux density at p1-p8 under the no-load condition with the  $F_c = 250 \text{ kA}\cdot\text{t}$ , it can be seen that the direct component of flux density at p1 is higher than that of the other points. Even if the value of the  $F_c$  changes, or the armature winding is fed by current, the flux density at p1 is always the biggest among the eight indicated points. So according to the aforementioned assumption (2), the maximum field current ( $I_{fmax}$ ) in the HTS coil is mainly determined by the flux density at p1. The waveform of flux density at p1 is shown in Figure 5(a), it can be seen that the armature reaction will slightly affect the flux density variation. Figure 5(b) shows the variation of the maximum flux density at p1 ( $B_{p1max}$ ) with  $F_c$  under the no-load and rated-load conditions, it can be seen that the flux density at p1 in the single-polarity one is approximately twice of that of the double-polarity one, meaning that the  $I_{fmax}$  in the HTS coil of double-polarity HTS-DSDDG will be much higher than that of the single-polarity HTS-DSDDG depending to the  $I_{fmax}$ - $B_{\perp}$  curve as shown in Figure 3.

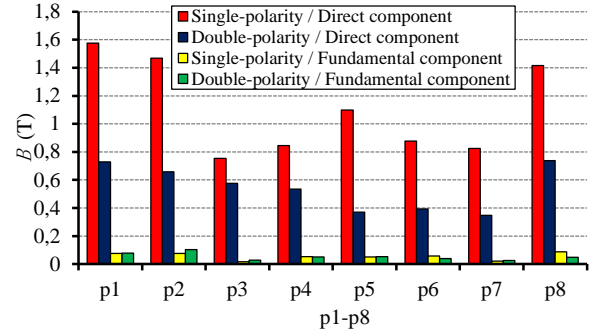


**Figure 4.** The direct component and fundamental component of flux density at p1-p8.

According to the above analysis, it can be found that the relationship curve between the  $I_{fmax}$  and the  $F_c$  can be derived from Figure 3 and Figure 5(a), as shown in Figure 6(a). the turn number per excitation pole-pair ( $N_f$ ) can be calculated by

$$N_f = \frac{F_c}{I_{fmax}} \quad (4)$$

Hence the relationship curve between the  $N_f$  and the  $F_c$  can be obtained as well, as shown in Figure 6(b). It can be seen that more HTS wires will be needed in the single-polarity HTS-DSDDG than the double-polarity HTS-DSDDG in the identical  $F_c$ .

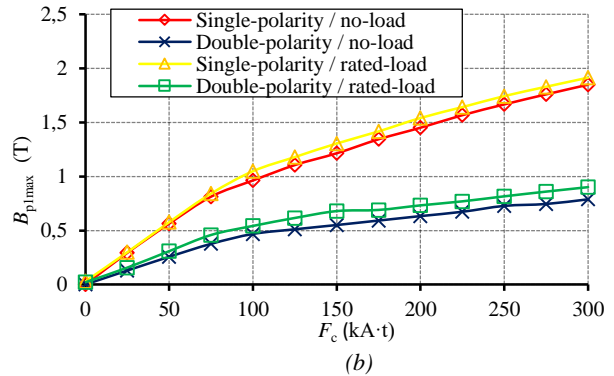
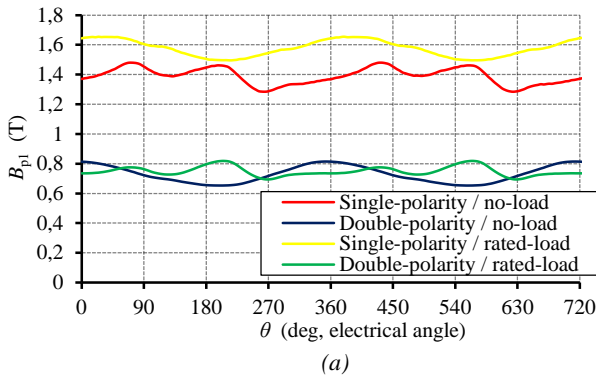


**Figure 5.** (a) Variation of flux density at p1 ( $B_{p1}$ ) with the rotor position ( $\theta$ , Elec. degree). (b) The variation of the maximum flux density at p1 ( $B_{p1max}$ ) with the excitation-MMF per excitation pole-pair ( $F_c$ ) under the no-load and rated-load conditions.

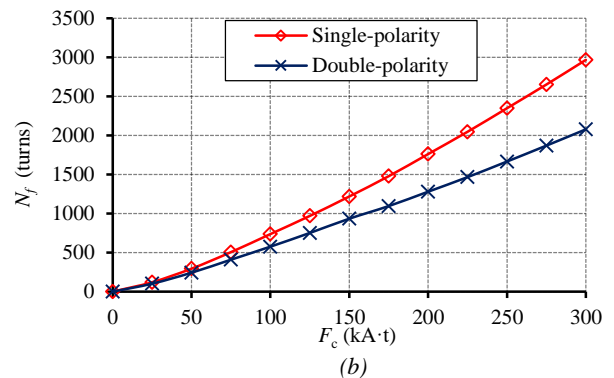
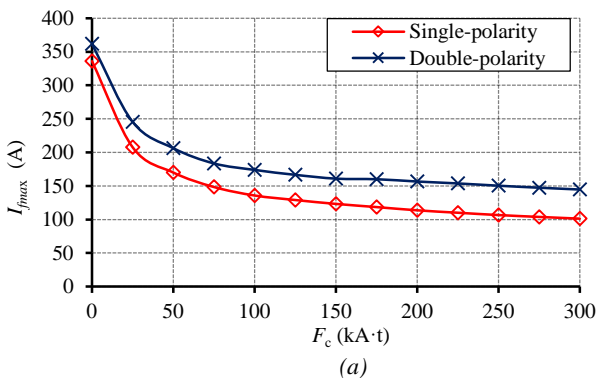


**Figure 6.** (a) Variation of the maximum field current in HTS coil ( $I_{fmax}$ ) with the excitation-MMF per excitation pole-pair ( $F_c$ ). (b) Variation of the turn number per excitation pole-pair ( $N_f$ ) with the  $F_c$ .

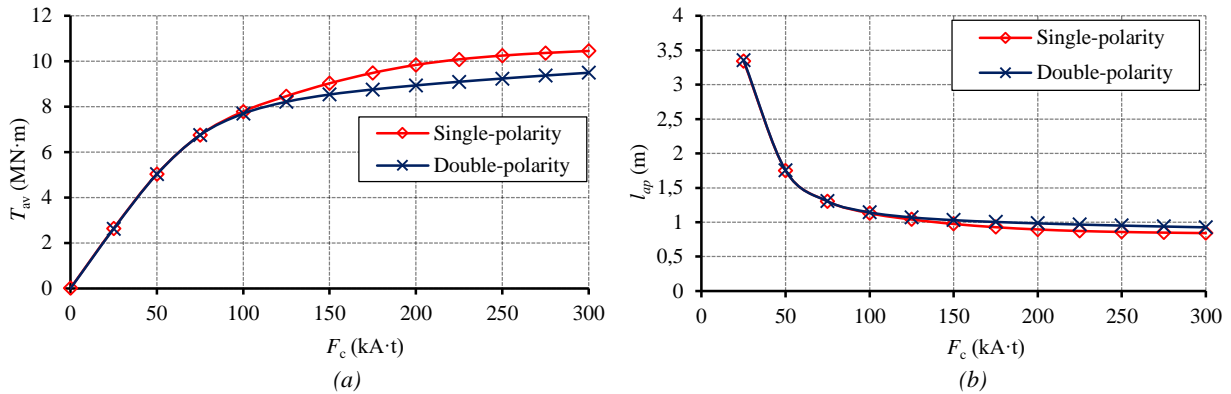


Figure 7. (a) Variation of the  $T_{av}$  with the  $F_c$ . (b) Variation of the  $l_{ap}$  with the  $F_c$ .

The relationship curve of the average electromagnetic torque ( $T_{av}$ ) and the  $F_c$  are shown in Figure 7(a) at the rated load with rotor axial length of 800 mm. It can be seen that the  $T_{av}$  of the double-polarity DSDDG becomes lower than that of the single-polarity one when  $F_c > 100$  kA·t, due to the fact that the width of inner-stator-teeth in the double-polarity one is relatively smaller than that of the single-polarity one, it prefers to become saturation to limit the flux density in the airgap. Then the rotor axial length ( $l_{ap}$ ) is adjusted to achieve an output power of 10 MW at the different  $F_c$ , relationship curve between which is shown in Figure 7(b).

The scaled-down sample of the racetrack-shaped HTS coil is shown in Figure 8 [30], which consists of two semicircles and two line-segments. So the length of HTS wire per excitation pole-pair ( $l_{HTS}$ ) is calculated by:

$$l_{HTS} = N_f \cdot (2\pi \frac{b_{mc}}{2} + 2l_{ap}) \quad (5)$$

where  $N_f$  is the turn number of per excitation pole-pair,  $b_{mc}$  is the width of middle turn of HTS coil.

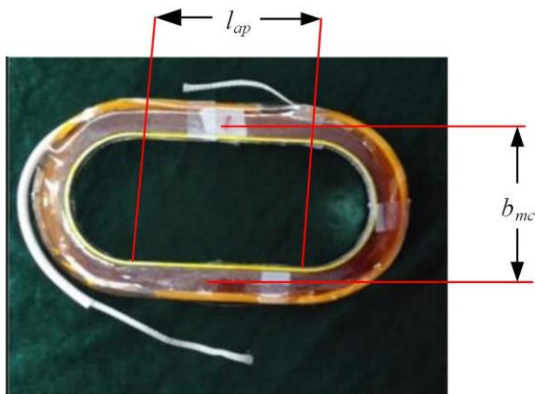


Figure 8. The scaled-down sample of the racetrack-shaped HTS coil.

Therefore, the relationship curve of the  $l_{HTS}$  and the  $l_{ap}$  can be derived from Figure 6(b), Figure 7(b), and Equation (5), as shown in Figure 9. It can be seen that the reduction of the  $l_{ap}$  is not linear with the increase of the  $l_{HTS}$ , there is a saturation between the  $l_{HTS}$  and the  $l_{ap}$ . At saturated region, it is difficult to reduce the volume of the

generators even with more quantities of HTS wires. Hence the  $l_{ap}$ - $l_{HTS}$  curve provides a criterion for selecting the appropriate excitation operating points. From the perspective of wind generator cost, the optimal excitation operating point should make wind generator has the lowest cost. However, the consumption of HTS wires is mainly concerning about the cost of HTS material, while the volume of wind generator will affect the material cost, the manufacturing cost, the transportation cost, and the installation cost. Therefore, the excitation operating point should be determined by the  $l_{ap}$ - $l_{HTS}$  curve and the specific production and application of the HTS-DSDDG for the objective of the lower cost.

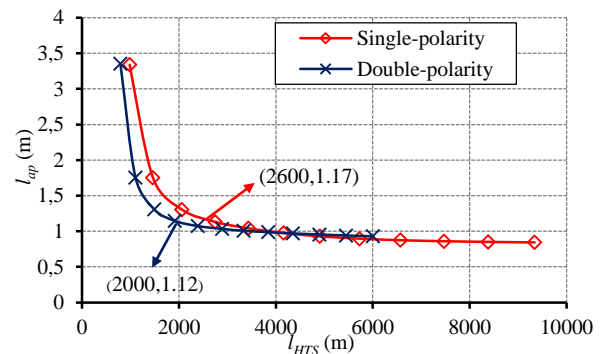


Figure 9. The relationship curve of the rotor axial length ( $l_{ap}$ ) and the length of HTS wire per excitation pole-pair ( $l_{HTS}$ ).

Table 2. The Selected excitation operating points for per excitation pole-pair

Parameter	Single-polarity	Double-polarity
$F_c$ (kA·t)	95	105
$I_{fmax}$ (A)	139	172
$N_f$ (turns)	683	610
$l_{ap}$ (mm)	1150	1130
$l_{HTS}$ (m)	2571	2011

In order to roughly compare the single-/double- polarity HTS-DSDDGs, the excitation operating points are selected at where the  $l_{ap}$ - $l_{HTS}$  curves are about to saturate, namely, point (2600,1.17) and (2000,1.12), corresponding to  $F_c=95$  kA·t and 105 kA·t, respectively, as shown in Figure 9. To reduce the calculation error, the

$l_{ap}$  will be slightly adjusted with fixed  $F_c$  to make the output power closer 10 MW. Finally, the excitation operating points of the single-/double-polarity DSDDGs are obtained, as listed in Table 2. It can be seen that the  $I_{fmax}$ , the  $l_{HTS}$ , and the  $l_{ap}$  of the double-polarity DSDDG is 23.7% higher, 21.8% lower, and 1.74% shorter than those of the single-polarity one, respectively.

## 4. COMPARISON OF THE TWO STRUCTURES

### 4.1. Comparison of Electromagnetic Performance

Since the excitation operating points of the single-/double-polarity HTS-DSDDGs are selected, their electromagnetic performance can be obtained and compared by FEA. Figure 10 illustrates the phase EMF waveforms under the no-load condition. It can be seen that both the EMF waveforms of single-/double-polarity HTS-DSDDGs are highly sinusoidal with amplitudes of approximate 3000 V, while the phase amplitudes of single-polarity HTS-DSDDG is 6.9 % higher than those of double-polarity HTS-DSDDG, probably due to its wider width of inner-stator-teeth compared to double-polarity HTS-DSDDG. The torque waveforms of the two generators at rated-load are shown in Figure 11. It can be found that both the two generators have the same  $T_{av}$  of 11 MN·m, while the torque ripple of single-polarity HTS-DSDDG is slightly larger than that of double-polarity of HTS-DSDDG.

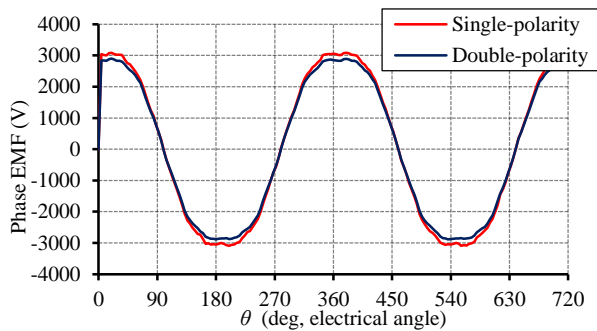


Figure 10. Phase EMF waveforms at no-load.

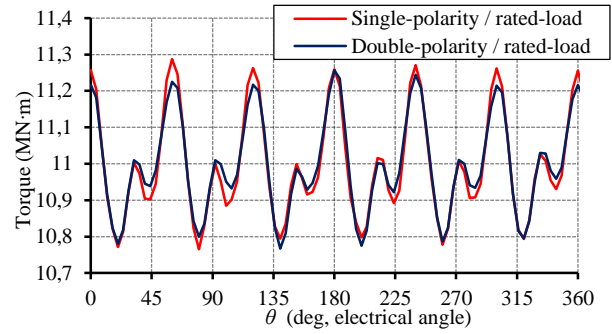


Figure 11. Torque waveforms at rated-load.

### 4.2. Comparison of Weight and Material Cost

After the selection of the excitation operating points, the volume and the HTS wire consumption of the two generators can be obtained as well, then their weights and material costs can be estimated and compared. The weight of the HTS-DSDDG include the structural and active materials masses, where the structural materials refer to rotor arm, stator arm, rotor cylinder, stator cylinder [31], and the active materials refer to copper, iron, dewar, HTS wires, cooling system. The material costs are determined by the masses and the unit costs. The masses and costs of dewar, cooling system and structural support are based on the reference of 10 MW MgB<sub>2</sub> SCDDG in [31].

The masses of the single-/double-polarity HTS-DSDDGs are presented in Table 3. It can be seen that the total masses of the single-/double-polarity DSDDGs are 461.6 tons and 437.9 tons, respectively, of which the structure support masses account for the largest proportion, 52.6 % and 54.2 % respectively, and the silicon steel masses are followed with 38.9 % and 36.6 %, respectively. Besides, it is worth noting that the total masses of the two generators are very close.

Referred to the current market price in China, the unit cost of materials used in the HTS-DSDDG are listed in Table 4. Then the material costs of the HTS-DSDDG components are obtained, as listed in Table 5. The total material costs of the single-/double-polarity DSDDGs are 2868.5 k\$ and 2835.3 k\$ respectively, of which the percentages of HTS wires are the maximum, 45.7 % and 37.5 %, respectively. Since the number of dewar in the double polarity HTS-DSDDG is double, its dewar cost is nearly twice of that of the single-polarity HTS-DSDDG. It can be seen that the total material cost of the double-polarity HTS-DSDDG is slightly lower than that of the single-polarity HTS-DSDDG, approximately 1.16 %.

Table 3. The masses of the single-/double-polarity HTS-DSDDGs

		Outer stator	Rotor	Inner stator	Copper windings	SC coil	Cooling system	Dewar	Structural support	Grand total
Single-polarity	Mass (ton)	61.8	26.9	90.9	25.6	8.3	1.8	3.6	242.8	461.6
	percentage	13.4%	5.8%	19.7%	5.5%	1.8%	0.4%	0.8%	52.6%	100%
Double-polarity	Mass (ton)	60.5	26.3	73.4	25.0	7.2	1.8	6.2	237.5	437.9
	percentage	13.8%	6.0%	16.8%	5.7%	1.6%	0.4%	1.4%	54.2%	100%

**Table 4.** The unit cost of materials

Material	Unit cost
Copper	11.6 \$/kg
Silicon steel	1.6 \$/kg
Structural steel	1.2 \$/kg
Bi-2223 wire	22 \$/m

**Table 5.** The material costs of the single-/double-polarity HTS-DSDDGs

		Outer stator	Rotor	Inner stator	Copper windings	SC coil	Cooling system	Dewar	Structural support	Grand total
Single-polarity	Material cost (k\$)	98.9	43.0	145.4	296.7	1361.7	233.0	398.5	291.3	2868.5
	percentage	3.4%	1.5%	5.1%	10.3%	47.5%	8.1%	13.9%	10.2%	100%
Double-polarity	Material cost (k\$)	96.8	42.1	117.4	290.3	1062.3	233.0	708.4	285.0	2835.3
	percentage	3.4%	1.5%	4.1%	10.2%	37.5%	8.2%	25.0%	10.1%	100%

## 5. CONCLUSION

In this paper, a method of selecting excitation operating point of HTS-DSDDG is proposed. The relationship of  $F_c$ ,  $I_{fmax}$ ,  $N_f$ ,  $T_{av}$ ,  $l_{ap}$ ,  $l_{HTS}$  are quantitatively investigated, then the  $l_{ap}$ - $l_{HTS}$  curves of single-/double-polarity HTS-DSDDG are obtained, which indicates the relationship between the HTS wires consumption and the volume of the generators, providing a criterion for selecting the optimal excitation operating point of the HTS-DSDDG to minimize the cost of wind generation. The different placement strategies of HTS coils lead to the different  $l_{ap}$ - $l_{HTS}$  curves. In order to compare the two structures, the excitation operating points are selected at where the  $l_{ap}$ - $l_{HTS}$  curves are about to saturate, then weight and material cost of the two HTS-DSDDGs are compared in detail. The comparison results reveal that the double-polarity 10 MW HTS-DSDDG has lighter weight and lower cost.

## ACKNOWLEDGEMENT

This work was supported in part by the NSFC under Project 51777216, in part by the Postgraduate Research & Practice Innovation Program of Jiangsu Province under Project KYCX18\_0092, and in part by the State Scholarship Fund of China Scholarship Council under Grant 201806090179.

## REFERENCES

- [1] Thang V. V., and Trung N. H., "Evaluating efficiency of renewable energy sources in planning micro-grids considering uncertainties", *Journal of Energy Systems*, 3(1): 14-25, (2019).
- [2] Naciri M., Aggour M., and Ahmed W. A., "Wind energy storage by pumped hydro station", *Journal of Energy Systems*, 1(1): 32-42, (2017).
- [3] Tan Z., Ngan H. W., Wu Y., et al., "Potential and policy issues for sustainable development of wind power in China", *Journal of Modern Power Systems and Clean Energy*, 1(3): 204-215, (2013).
- [4] Balat M., "A review of modern wind turbine technology", *Energy Sources, Part A: Recovery, Utilization, and Environmental Effects*, 31(17): 1561-1572, (2009).
- [5] Bilgili M., Yasar A., and Simsek E., "Offshore wind power development in Europe and its comparison with onshore counterpart", *Renewable and Sustainable Energy Reviews*, 15(2): 905-915, (2011).
- [6] Perveen R., Kishor N., and Mohanty S. R., "Off-shore wind farm development: Present status and challenges", *Renewable and Sustainable Energy Reviews*, 29: 780-792, (2014).
- [7] Global Wind Energy Council Report, "Global wind report 2018", April 2019.
- [8] The European Wind Association Report, "Offshore Wind in Europe – Key Trends and Statistics 2018", February 2019.
- [9] Roland Berger Strategic Consultants Report, "Offshore Wind Toward 2020-on the Pathway to Cost Competitiveness", April 2013.
- [10] Natarajan A., "An overview of the state of the art technologies for multi-MW scale offshore wind turbines and beyond", *Wiley Interdisciplinary Reviews: Energy and Environment*, 3(2): 111-121, (2014).
- [11] Bensalah A., Benhamida M. A., Barakat G., et al., "Large wind turbine generators: State-of-the-art review", 2018 XIII International Conference on Electrical Machines (ICEM), Alexandroupoli, Greece, 2205–2211, (2018).
- [12] Cheng M. and Zhu Y., "The state of the art of wind energy conversion systems and technologies: A review", *Energy Conversion and Management*, 88: 332-347, (2014).
- [13] McKenna R., Ostman v.d. Leye P., and Fichtner W., "Key challenges and prospects for large wind turbines", *Renewable and Sustainable Energy Reviews*, 53: 1212-1221, (2016).
- [14] Polinder H., Pijl F. F. A. van der., Vilder G.- de., et al. "Comparison of direct-drive and geared generator concepts for wind turbines", *IEEE Transactions on Energy Conversion*, 21(3): 725-733, (2006).
- [15] Fair R., Stautner W., Douglass M., et al., "Superconductivity for Large Scale Wind Turbines", General Electric - Global Research, United States, (2012).
- [16] Bray J. W., "Application of superconducting materials to power equipment", *Journal of Electronic Materials*, 24(12): 1767-1772, (1995).
- [17] Zhu X., and Cheng M., "Design and analysis of 10 MW class HTS exciting double stator direct-drive wind generator with stationary seal", *IEEE Access*, 7: 51129-51139, (2019).
- [18] Qu R., Liu Y., and Wang J., "Review of superconducting generator topologies for direct-drive wind turbines", *IEEE Transactions on Applied Superconductivity*,

- 23(3): 5201108-5201108, (2013).
- [19] Maples B., Hand M., and Musial W., "Comparative Assessment of Direct Drive High Temperature Superconducting Generators in Multi-Megawatt Class Wind Turbines", National Renewable Energy Lab. (NREL), Golden, CO (United States), (2010).
- [20] Marino I., Pujana A., Sarmiento G., et al., "Lightweight MgB<sub>2</sub> superconducting 10 MW wind generator", *Superconductor Science and Technology*, 29(2): 024005-024005, (2015).
- [21] Wang J., Qu R., Tang Y., et al., "Design of a superconducting synchronous generator with LTS field windings for 12 MW offshore direct-drive wind turbines", *IEEE Transactions on Industrial Electronics*, 63(3): 1618-1628, (2016).
- [22] Cheng Y., Li D., Kong W., et al., "Electromagnetic design of a large-scale double-stator direct driving HTS wind generator", *IEEE Transactions on Applied Superconductivity*, 28(4): 1-5, (2018).
- [23] Abrahamsen A. B., Mijatovic N., Seiler E., et al., "Superconducting wind turbine generators", *Superconductor Science and Technology*, 23(3): 034019-034019, (2010).
- [24] Snitchler G., Gamble B., King C., et al., "10 MW class superconductor wind turbine generators", *IEEE Transactions on Applied Superconductivity*, 21(3): 1089-1092, (2011).
- [25] Xu Y., Maki N., and Izumi M., "Overview study on electrical design of large-scale wind turbine HTS generators", *IEEE Transactions on Applied Superconductivity*, 28(5): 1-5, (2018).
- [26] Lloberas J., Sumper A., Sanmarti M., et al., "A review of high temperature superconductors for offshore wind power synchronous generators", *Renewable and Sustainable Energy Reviews*, 38: 404-414, (2014).
- [27] Abrahamsen A. B., Magnusson N., Jensen B. B., et al., "Large superconducting wind turbine generators", *Energy Procedia*, 24: 60-67, (2012).
- [28] Cheng M., Han P., and Hua W., "General airgap field modulation theory for electrical machines", *IEEE Transactions on Industrial Electronics*, 64(8): 6063-6074, (2017).
- [29] Wang Y., Feng Q., Li X., and Ma W., "Design, analysis and experimental test of a segmented-rotor high temperature superconducting flux-switching generator with stationary seal", *IEEE Transactions on Industrial Electronics*, 65(11):9047-9055, (2018).
- [30] Wang Y., Yang G., Zhu X., Lin X., and Ma W., "Electromagnetic characteristics analysis of a high-temperature superconducting field-modulation double-stator machine with stationary seal", *Energies*, 11(5): 1269-1269, (2018).
- [31] Polinder H., "Final assessment of superconducting (SC) and pseudo direct drive (PDD) generator performance indicators (PI's)", DTU wind, FP7-ENERGY-2012-1-2STAGE, INNWIND.EU, Tech. Rep., Deliverable D3.44, (2017).